Interface Elements in Global/Local Analysis – Part 2: Surface Interface Elements

John E. Schiermeier
Senior Development Engineer
The MacNeal–Schwendler Corporation
Los Angeles, California

Jerrold M. Housner
Jonathan B. Ransom
NASA Langley Research Center
Hampton, Virginia

Mohammad A. Aminpour
Applied Research Associates, Inc.
Hampton, Virginia

W. Jefferson Stroud
NASA Langley Research Center
Hampton, Virginia

The 1997 MSC Aerospace Users' Conference
Newport Beach, California
November 17–20, 1997

Abstract

When performing global/local analysis, the issue of connecting dissimilar meshes often arises, especially when refinement is performed. One method of connecting these dissimilar meshes is to use interface elements. In the previous Part 1, curve interface elements, implemented in MSC/NASTRAN Version 69 for shell and beam p–element edges, were presented. In the current Part 2, surface interface elements, being implemented in MSC/NASTRAN for solid and shell p–element faces, are presented with examples.

1. Introduction

The problem of connecting dissimilar meshes at a common interface is a major one in finite element analysis. One method of connecting these dissimilar meshes is to use interface elements.

The previous paper, Part 1 [1], described the curve interface elements implemented in Version 69 of MSC/NASTRAN for shell and beam p–element edges. The background, theory, implementation, and examples were also presented. The current paper, Part 2, describes the surface interface elements being implemented in MSC/NASTRAN for solid and shell p–element faces. The background, theory, and implementation are very similar to Part 1 [1] and will be repeated and extended here. Examples will also be presented.

1.1. Applications

Dissimilar meshes can occur with global/local analysis, where part of the structure is modeled as the area of primary interest, in which detailed stress distributions are required, and part of the structure is modeled as the area of secondary interest, through which load paths are passed into the area of primary interest. Generally the area of primary interest has a finer mesh than the area of secondary interest, and therefore a transition area is required. Severe transitions generally produce elements that are heavily distorted, which can result in poor stresses and poor load transfer into the area of primary interest. Patches of elements may be removed from the global model and replaced by a denser patches for local detail. An example is shown in Figure 1, where the boundaries of the patches are bold.

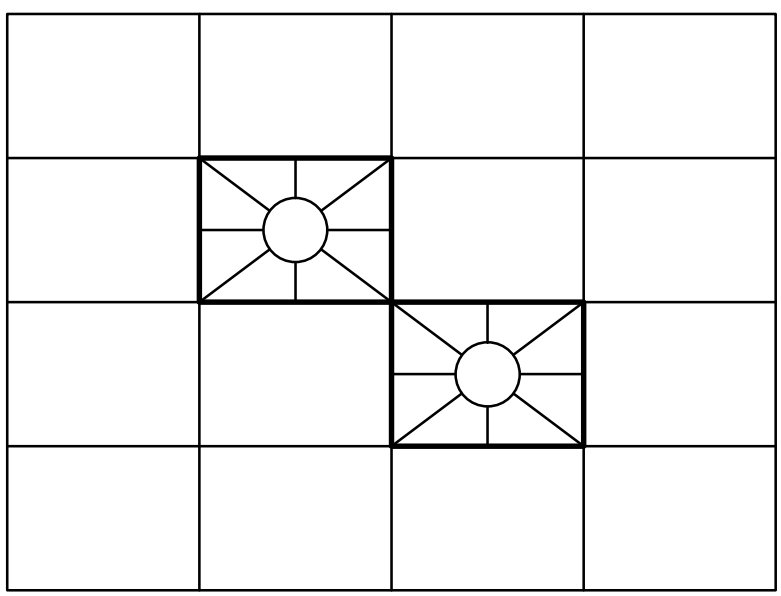

Figure 1: Example of Dissimilar Mesh from Global/Local Analysis.

In large system problems, different analysts or even different organizations may have created different components of the model, such as the wing and the fuselage of an airplane. Unless they have carefully coordinated their efforts, the finite element meshes of the different components may not match at the interfaces, as otherwise required, when they are assembled.

Dissimilar meshes can arise with automeshers, which may be required to transition between large elements and small elements in a limited area. An example is shown in Figure 2, where the boundary is bold and the required transition is dashed. Many automeshers generate tetrahedral meshes for solids, and distorted tetrahedra may be more susceptible to poor results. Automeshers are often used in conjunction with shape optimization procedures, where the shape changes are large enough to warrant remeshing. In these cases, it would be more efficient to remesh only the local part of the model and interface it with the rest, rather than remeshing the entire model. If the rest of the model has not been remeshed, then the associated parts of the stiffness matrix need not be recalculated, provided that the previous data has been saved.

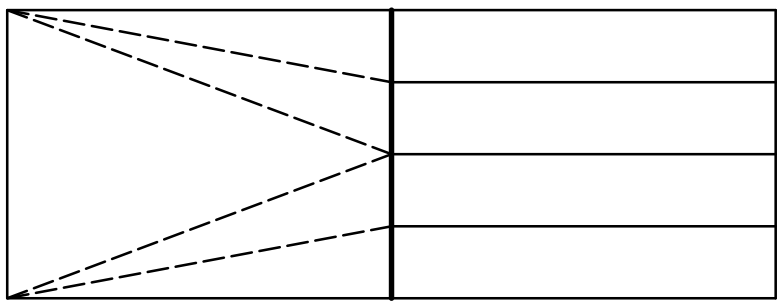

Figure 2: Example of Dissimilar Mesh from Automesher.

In h–refinement, subdivided elements may be adjacent to undivided elements. Without some kind of interface element, the subdivision would have to be carried out to the model boundary or otherwise phased out. An example is shown in Figure 3, where the boundary is bold and the required transitions are dashed.

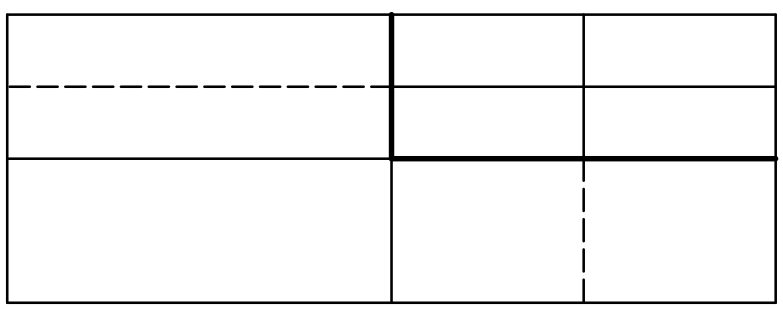

Figure 3: Example of Dissimilar Mesh from h–Refinement.

1.2. Previous Methods

Much work has been done to resolve the element interface problem, with most of the efforts concentrating on moving the nodes or writing multi–point constraint (MPC) equations on the interfaces. The first approach, moving the nodes, must take into account the element distortions on both sides of the interface and provide the best redistribution according to some criteria. However, it is possible that one or both sides of the interface may be represented only by previously–generated stiffness matrices, in which case the nodes cannot be moved. The biggest restriction of moving nodes is that both sides of the interface must have the same number and type of elements. Therefore, this method is not practical for the general problem.

The second approach, using MPC equations, often is used for connecting elements of different types. For example, the midside node of a quadratic element may be constrained to move linearly with the vertex nodes in order to match an adjacent linear element, assuming that the vertex nodes for the two elements are coincident. Other MPC equations, such as splines, can handle more general cases. However, MPC equations by definition provide additional relationships for the existing degrees of freedom on the interface, and in the process reduce the number of independent degrees of freedom. If there are no degrees of freedom created, this could result in additional local stiffness or other non–physical effects in the model.

1.3. Current Method

The need and applications for reliable interface technology are great. NASA Langley Research Center has developed a method for analyzing structures composed of two or more independently modeled substructures, based on a hybrid variational formulation with Lagrange multipliers, and applied it to global/local demonstration problems for one–dimensional [2–5] and two–dimensional [6] interfaces.

Under terms of a cooperative agreement between MSC and NASA [7], MSC has implemented this technology into MSC/NASTRAN for shell and beam p–element edges along a geometric curve, and is implementing the technology for solid and shell p–element faces over a geometric surface. This agreement is part of NASA's continuing effort to transfer technology into the mainstream of industry as an aid in developing competitiveness in the worldwide market.

2. Formulation

The formulation of the interface element, which is a hybrid variational formulation using Lagrange multipliers, is defined in summary as follows, using primarily the notation in [2]. It is repeated in more general form here to include the dynamic case. The complete details for the static case may be found in [2–4,6].

The displacement vector $\{v\}$ on the interface is defined in terms of the node, edge, and face coefficients $\{q_s\}$, which are defined on the interface elements, and interpolation functions $[T]$, which is a matrix containing the functions for each field of the interface displacement vector:

$$\{v\} = [T]\{q_s\}$$

The displacement vector $\{u_j\}$ on each subdomain j is defined in terms of the node, edge, and face coefficients $\{q_j\}$ and interpolation functions $[N_j]$, which is a matrix containing the functions for each field of the subdomain displacement vector:

$$\{u_j\} = [N_j]\{q_j\}$$

The Lagrange multiplier vector $\{\lambda_j\}$ on each subdomain j is defined in terms of the node, edge, and face coefficients $\{\alpha_j\}$ and interpolation functions $[R_j]$, which is a matrix containing the functions for each field of the Lagrange multiplier vector:

$$\{\lambda_j\} = [R_j]\{\alpha_j\}$$

Defining the combined operator and material matrix $[B_j]$, the density ρ, and the surface tractions $\{t_j\}$; and considering the potential energy for all the subdomains j with the internal energy, inertial forces, and applied forces, and for the interface I with the Lagrange multipliers gives:

$$\Pi = \sum_j \left[\frac{1}{2}\int_\Omega u_j^T\ B_j\ u_j\ dV + \frac{1}{2}\int_\Omega u_j^T\ \rho_j\ \ddot{u}_j\ dV - \int_\Gamma u_j^T\ t\ dA + \int_I \lambda_j^T\ (v - u_j)\ dA \right]$$

where the inertial body forces:

$$F_j = -\rho_j\ \ddot{u}_j$$

have been multiplied by a factor of one half since they are proportional loads. Using the standard assumption of simple harmonic motion for the frequency ω:

$$\ddot{u}_j = -\omega^2\ u_j$$

and expanding the vectors into their coefficients and interpolation functions gives:

$$\Pi = \sum_j \left[\frac{1}{2}\int_\Omega q_j^T\ N_j^T\ B_j\ N_j\ q_j\ dV - \frac{1}{2}\int_\Omega q_j^T\ N_j^T\ \rho_j\ \omega^2\ N_j\ q_j\ dV - \int_\Gamma q_j^T\ N_j^T\ t_j\ dA \right.$$
$$\left. + \int_I \left(q_s^T\ T^T - q_j^T\ N_j^T\right) R_j\ \alpha_j\ dA \right]$$

Defining the matrices of interpolation functions:

$$M_j = -\int_I N_j^T\ R_j\ dA$$

$$G_j = \int_I T^T\ R_j\ dA$$

and substituting these, together with the standard definition of stiffness matrices $[k_j]$, mass matrices $[m_j]$, and load vectors $\{f_j\}$, into the potential energy gives:

$$\Pi = \sum_j \left[\frac{1}{2} q_j{}^T \; k_j \; q_j - \frac{1}{2}\omega^2 q_j{}^T \; m_j \; q_j - q_j{}^T \; f_j + \left(q_s{}^T \; G_j + q_j{}^T \; M_j \right) \alpha_j \right]$$

Partitioning the q into q^i, those node, edge, and face coefficients on the interface, and q^o, those coefficients other than on the interface, gives:

$$\Pi = \sum_j \left\{ \frac{1}{2} \left\lfloor q_j^{o\,T} \;\; q_j^{i\,T} \right\rfloor \begin{bmatrix} k_j^{oo} & k_j^{oi} \\ k_j^{io} & k_j^{ii} \end{bmatrix} \begin{Bmatrix} q_j^o \\ q_j^i \end{Bmatrix} - \frac{1}{2}\omega^2 \left\lfloor q_j^{o\,T} \;\; q_j^{i\,T} \right\rfloor \begin{bmatrix} m_j^{oo} & m_j^{oi} \\ m_j^{io} & m_j^{ii} \end{bmatrix} \begin{Bmatrix} q_j^o \\ q_j^i \end{Bmatrix} \right.$$

$$\left. - \left\lfloor q_j^{i\,T} \;\; q_j^{o\,T} \right\rfloor \begin{Bmatrix} f_j^i \\ f_j^o \end{Bmatrix} + \left(\lfloor q_s{}^T \rfloor \; [G_j] + \lfloor q_j^{i\,T} \rfloor \; [M_j] \right) \{\alpha_j\} \right\}$$

Deriving the Euler equations by taking the variations of the potential energy with respect to the four groups of variables $q_j{}^o$, $q_j{}^i$, q_s, and α_j gives:

$$\frac{\partial \Pi}{\partial q_j^o} = \left(k_j^{oo} - \omega^2 \; m_j^{oo} \right) q_j^o + \left(k_j^{oi} - \omega^2 \; m_j^{oi} \right) q_j^i - f_j^o = 0$$

$$\frac{\partial \Pi}{\partial q_j^i} = \left(k_j^{io} - \omega^2 \; m_j^{io} \right) q_j^o + \left(k_j^{ii} - \omega^2 \; m_j^{ii} \right) q_j^i - f_j^i + M_j \; \alpha_j = 0$$

$$\frac{\partial \Pi}{\partial q_s} = \sum_j G_j \; \alpha_j = 0$$

$$\frac{\partial \Pi}{\partial \alpha_j} = G_j{}^T \; q_s + M_j{}^T \; q_j^i = 0$$

Each of the Euler equations has a physical interpretation. Writing the Euler equations in matrix form:

$$\left(\begin{bmatrix} k_j^{oo} & k_j^{oi} & \dots & 0 & 0 & \dots \\ k_j^{io} & k_j^{ii} & \dots & 0 & M_j & \dots \\ \vdots & \vdots & & \vdots & \vdots & \\ 0 & 0 & \dots & 0 & G_j & \dots \\ 0 & M_j{}^T & \dots & G_j{}^T & 0 & \dots \\ \vdots & \vdots & & \vdots & \vdots & \end{bmatrix} - \omega^2 \begin{bmatrix} m_j^{oo} & m_j^{oi} & \dots & 0 & 0 & \dots \\ m_j^{io} & m_j^{ii} & \dots & 0 & 0 & \dots \\ \vdots & \vdots & & \vdots & \vdots & \\ 0 & 0 & \dots & 0 & 0 & \dots \\ 0 & 0 & \dots & 0 & 0 & \dots \\ \vdots & \vdots & & \vdots & \vdots & \end{bmatrix} \right) \begin{Bmatrix} q_j^o \\ q_j^i \\ \vdots \\ q_s \\ \alpha_j \\ \vdots \end{Bmatrix} = \begin{Bmatrix} f_j^o \\ f_j^i \\ \vdots \\ 0 \\ 0 \\ \vdots \end{Bmatrix}$$

This system of equations is symmetric, but not positive definite. All of the interface terms $[M_j]$ and $[G_j]$ appear in the stiffness matrix, with none in the mass matrix. Had damping been included, which generally takes the form of a load proportional to the velocity, the result would have been similar.

3. Implementation

Three new bulk data entries, GMBNDS (Geometric Boundary – Surface), GMINTS (Geometric Interface – Surface), and PINTS (Properties of Geometric Interface – Surface), have been implemented for specifying the surface interface elements. These entries define the subdomain boundaries, the interface elements, and the interface element properties, respectively. Detailed information on the input data will be available in [8].

Currently there are three methods of defining the subdomain boundaries of solid or shell p–element faces, as shown in Figure 4. For the surface interface, each boundary may be defined using the GMSURF with which the finite element faces are associated; the FEFACEs defining the finite element faces; or in the most basic form, the GRIDs over the finite element faces.

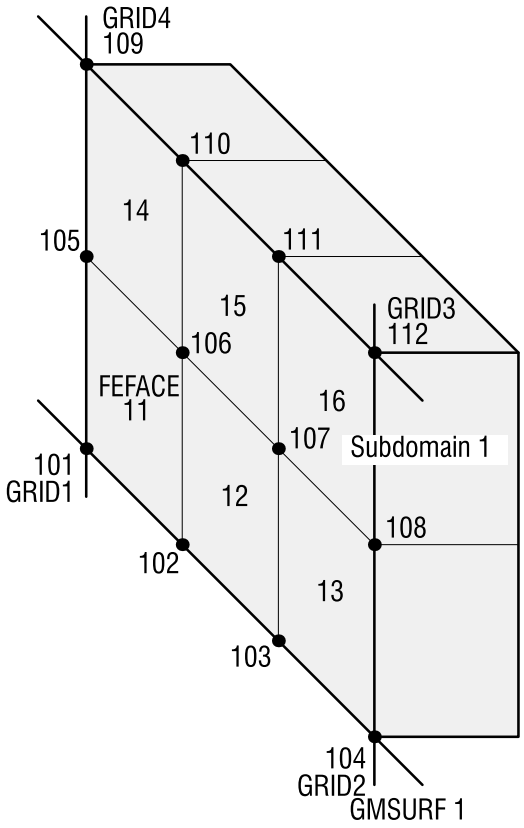

Figure 4: Surface Boundary Definition.

Once the boundaries have been defined, they must be associated with the interface elements, as shown in Figure 5. This is accomplished by referencing the boundaries in the interface element definition.

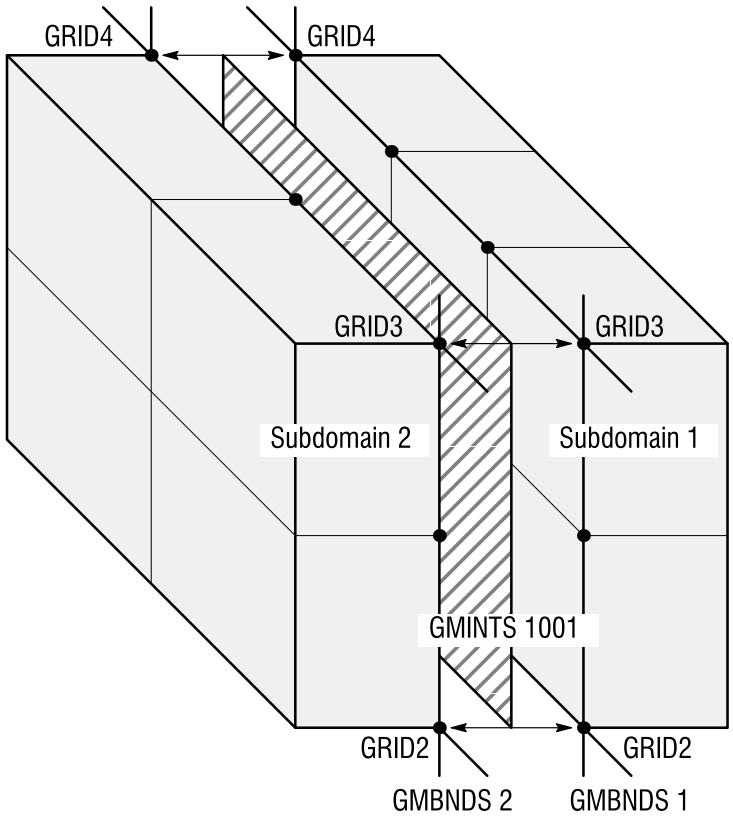

Figure 5: Surface Interface Element Definition (exploded view).

Since the interface elements consist only of the differences in displacement components weighted by the Lagrange multipliers, there are no conventional element or material properties. The property bulk data entry specifies a tolerance for the interface elements, which defines the allowable distance between the subdomain boundaries; and a scaling factor, which may improve the conditioning of the Lagrange multipliers.

4. Example Problems

Several sets of example problems were analyzed, in order to test the capabilities of the interface elements with various boundary meshes. The goal of the interface element is that it should not decrease the accuracy below that obtained using the less refined boundary with a conforming mesh. However, it will not increase the accuracy above that obtained using the more refined boundary with a conforming mesh. For example, if one boundary had a single element face and the other had several element faces at a given p–level, the accuracy with the interface elements should fall between a similar problem with two conforming single–face boundaries and a similar problem with two conforming multiple–face boundaries.

4.1. Cantilever Beam

The first set of example problems used a cantilever beam that had exact solutions at low p–levels. The boundaries for each of the six meshes are shown in Figure 6; each boundary corresponds to a cross section of the cantilever beam. The first mesh, one hexa/one hexa, served as a baseline for the interface and used an interface element, even though it is a conforming configuration.

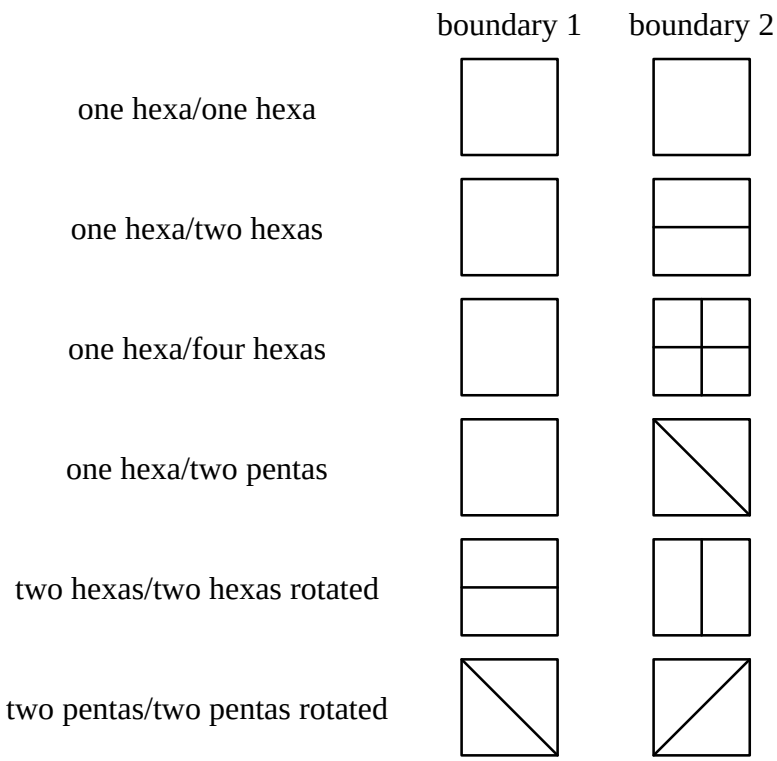

Figure 6: Boundaries on Cantilever Beams.

Tension (exact at p=1), moment (exact at p=2), and shear (exact at p=3) load cases were analyzed. The von Mises stress contours at p=3 for all three of these load cases with the two pentas/two pentas rotated mesh are shown on the deformed shape in Figure 7. The maximum stress values are also printed at the appropriate locations. Note that the variations in the tension case are due to the very small contour range; the actual range of values is 9.988 to 10.02.

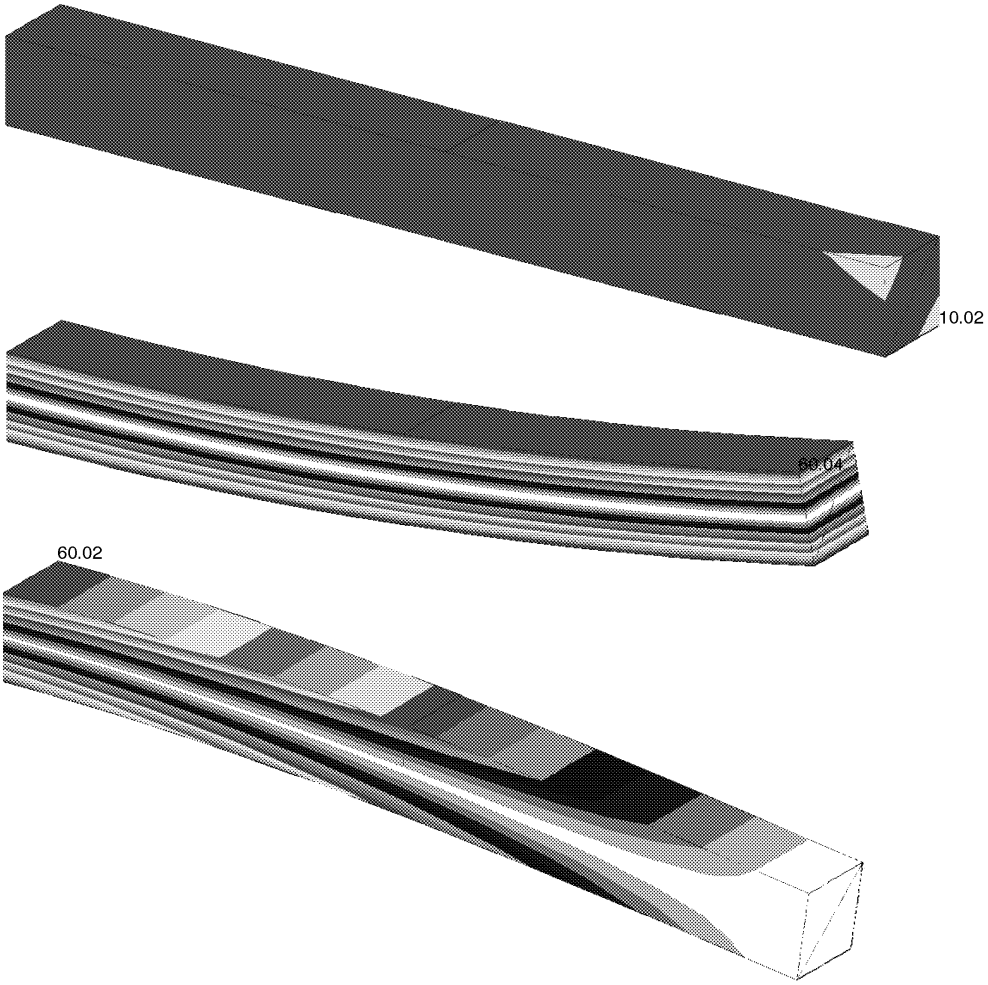

Figure 7: Stress Contours on Cantilever Beam (p=3).

The maximum values of the von Mises stress at p=3 for the three load cases are listed in Table 1 for all six meshes. The first mesh is exact, since it is conforming, and none of the other meshes differ from the exact solution by more than 1%. Since the load cases have exact solutions at low p–levels, all of the meshes should be exact. The reason for the differences is that the element shape functions are only C^0 continuous across element boundaries, and therefore can not be integrated exactly unless the integrations are done in a piecewise manner. Additional integration points make the solution more accurate, but only the piecewise integration would make it exact. This would add significant overhead to the surface interface elements.

Table 1: Maximum Stress for Cantilever Beam (p=3).

mesh	tension (von Mises)	moment (von Mises)	shear (von Mises)
one hexa/one hexa	10.00	60.00	60.00
one hexa/two hexas	10.05	60.00	60.00
one hexa/four hexas	10.10	60.25	60.09
one hexa/two pentas	10.02	60.01	60.01
two hexas/two hexas rotated	10.05	60.25	60.09
two pentas/two pentas rotated	10.02	60.04	60.02

4.2. Circular Shaft

The second set of example problems is a circular shaft that has exact solutions at low p–levels. The boundaries for the two meshes are shown in Figure 8. Again, the first mesh is a conforming mesh that serves as a baseline.

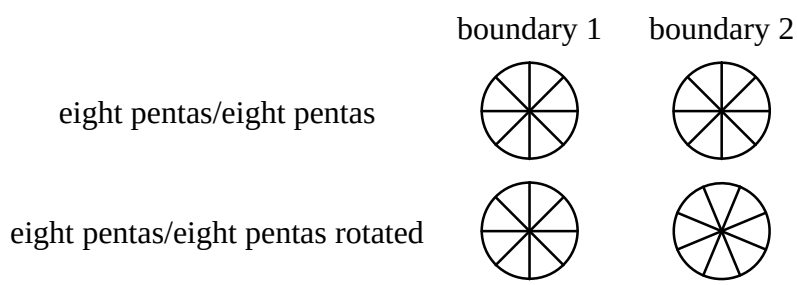

Figure 8: Boundaries on Circular Shafts.

Tension (exact at p=1) and torsion (exact at p=3) load cases were analyzed. The max principal stress contours for the tension case and the max shear stress contours for the torsion case at p=3 for the eight pentas/eight pentas rotated mesh are shown on the deformed shape in Figure 9. The maximum stress values are also printed at the appropriate locations. Note that the variations in the tension case are due to the very small contour range; the actual range of values is 9.995 to 10.00.

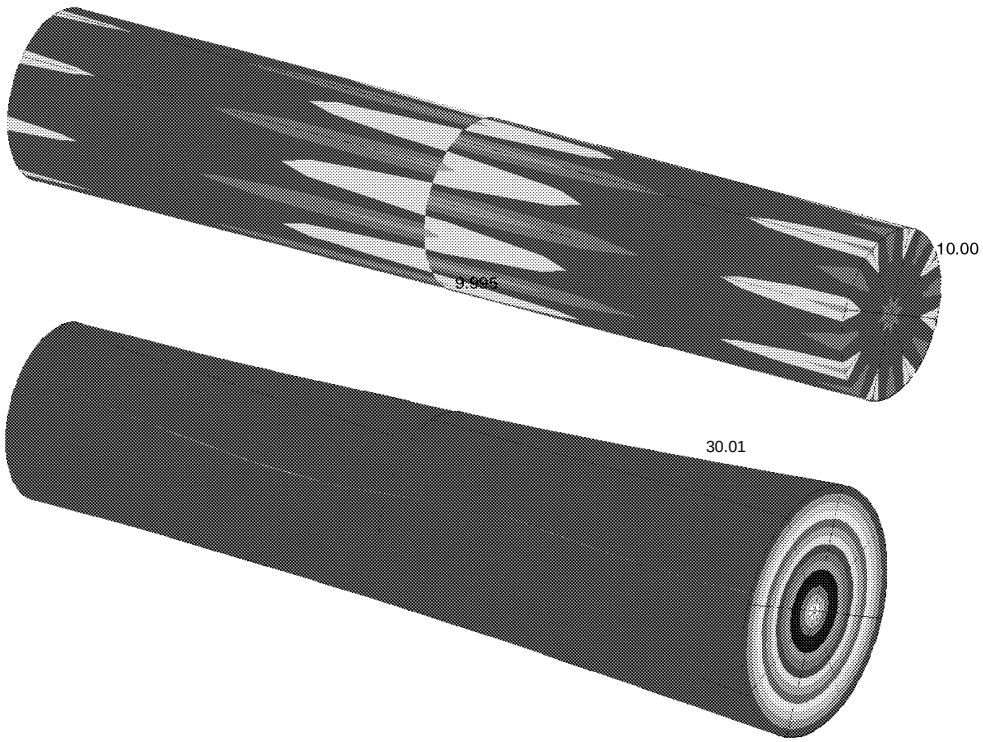

Figure 9: Stress Contours on Circular Shaft (p=3).

The maximum stress values at p=3 for the three load cases are listed in Table 2 for both meshes. The first mesh is exact, since the mesh is conforming, and the other mesh differs from the exact solution by less than 0.1%.

Table 2: Maximum Stress on Circular Shaft (p=3).

mesh	tension (max principal)	torsion (max shear)
eight pentas/eight pentas	10.00	30.00
eight pentas/eight pentas rotated	10.00	30.01

4.3. Scordelis–Lo Roof

The third example problem is the Scordelis–Lo roof [9], which includes curvature in the interface elements. One mesh is shown in Figure 10, where one boundary consists of two hexa elements, and the other boundary consists of four hexa elements. (Note that this particular mesh refinement is not the most advantageous, but is being used to illustrate the interface elements.)

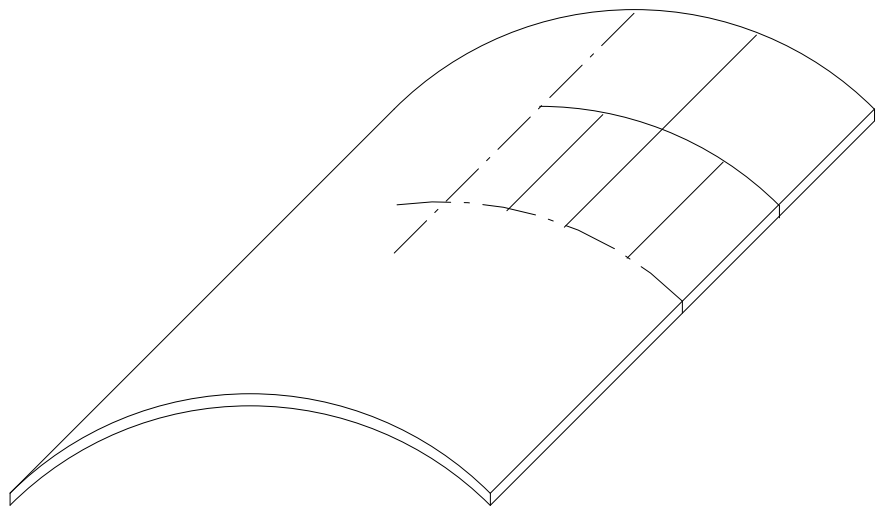

Figure 10: Scordelis–Lo Roof.

The roof has simple supports on the curved ends and is loaded by its own weight. Using symmetry constraints, only a quarter of the model was analyzed. The vertical displacement contours for the two hexa/four hexa mesh are shown on the deformed shape in Figure 11.

The vertical displacements at the midside of the free side at p=8 are listed in Table 3 for four meshes with interface elements. All of the meshes have the same displacement of –0.2973. The value cited in [9] is –0.3086, with the notation that many elements converge to a lower value such as –0.3024. However, that value is for shell elements, which have assumptions of the general continuum theory used by solid elements. The simply–supported boundary conditions are also not equivalent for solid elements.

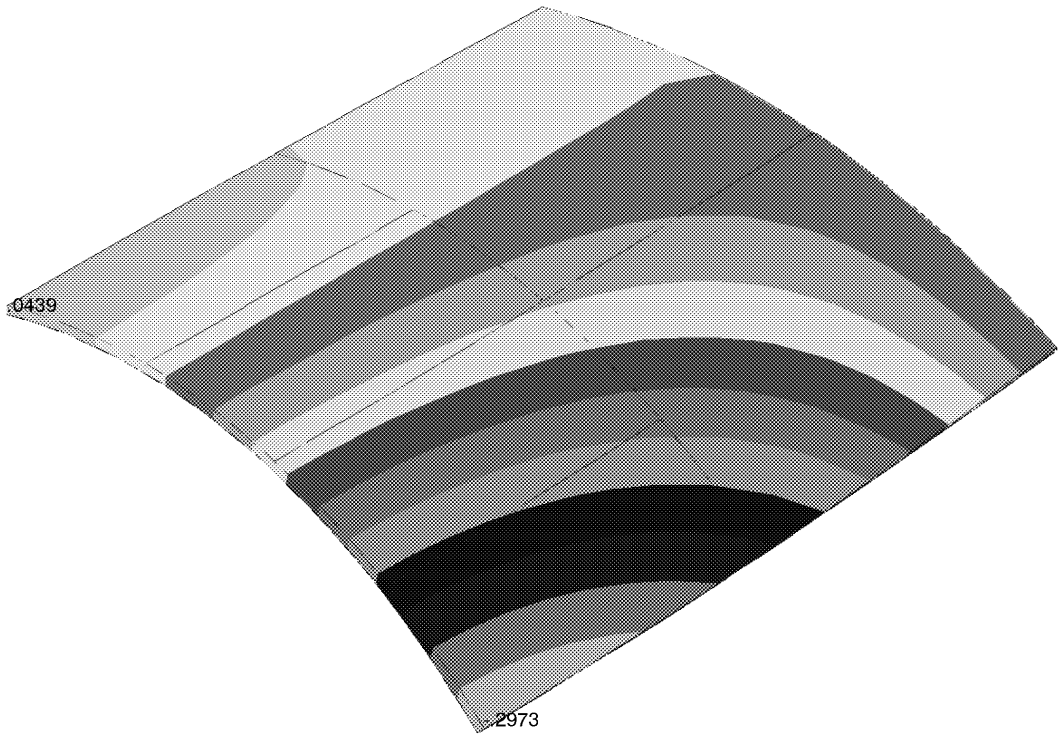

Figure 11: Displacement Contours on Scordelis–Lo Roof (p=8).

Table 3: Midside Displacement on Scordelis–Lo Roof (p=8).

Mesh	Displacement (vertical)
two hexas/two hexas	–0.2973
two hexas/three hexas	–0.2973
two hexas/four hexas	–0.2973
four hexas/four hexas	–0.2973

4.4. Square Plate with Circular Hole

The fourth example problem is a square plate with a circular hole, as shown in Figure 12. The hole is small enough relative to the plate that additional elements, though not necessary, greatly improve convergence. This example better illustrates how a global/local problem could be modeled, since the patch of elements around the hole was replaced without modifying the mesh away from the hole.

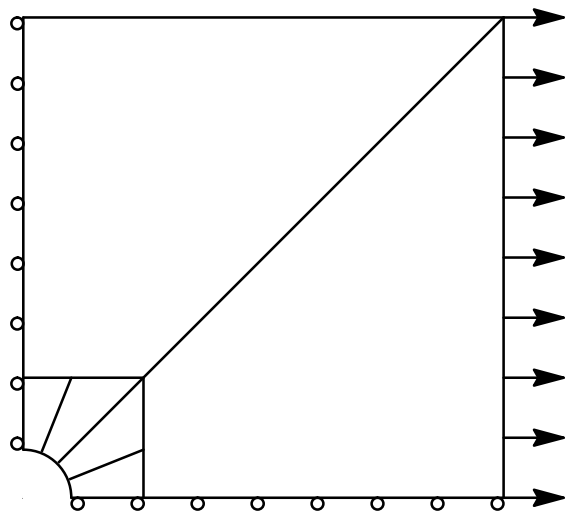

Figure 12: Square Plate with Circular Hole.

The square plate has a uniform tension load, so that the stress concentration factor at the hole may be calculated, and symmetry constraints. Two interface elements were used, since the interface contains a right angle. The von Mises stress contours for the two hexa/four hexa mesh are shown on the deformed shape in Figure 13. The boundary between the large light and dark areas in the figure has a contour value of exactly the applied stress of 10.00, such that any minutely small differences from the applied stress are shown.

The stress concentration factors at p=8 are listed in Table 4 for four meshes with interface elements. Values are listed for both the middle surface and the top surface in order to show the variation through the thickness. The value calculated from [10] for a semi–infinite plate is 2.72, which is derived from curve fits to photoelastic data for a specified accuracy of much less than 5%. After the simplest mesh, the results are identical at 2.81 on the middle surface and 2.65 on the top surface. The highest factor occurs at the middle surface of the model, which is slightly higher than the plate solution, whereas the factor on the top and bottom surfaces is slightly lower, due to the Poisson effect.

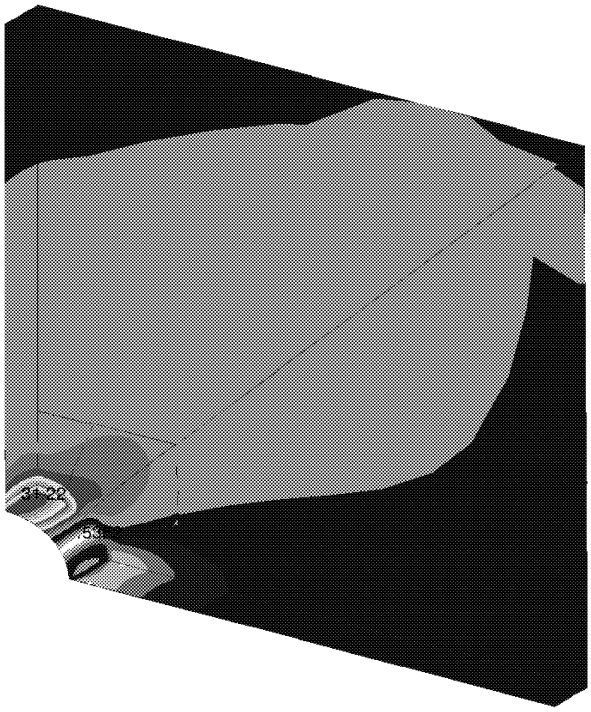

Figure 13: Stress Contours on Plate with Hole (p=8).

Table 4: Stress Concentration Factors for Plate with Hole (p=8).

Mesh	Stress Concentration (middle surface)	Stress Concentration (top surface)
two hexas/two hexas	2.796	2.647
two hexas/three hexas	2.810	2.654
two hexas/four hexas	2.810	2.655
four hexas/four hexas	2.810	2.654

5. Conclusions

Interface elements for dissimilar meshes are being implemented in MSC/NASTRAN. In the previous Part 1 [1], curve interface elements for shell and beam p–element edges along a geometric curve were presented; in the current Part 2, surface interface elements for solid and shell p–element faces over a geometric surface are being presented. These elements are applicable to a wide range of problems, such as global/local analysis and component assembly. The interface elements use the hybrid variational formulation developed by NASA, which was summarized in this paper along with the implementation in MSC/NASTRAN.

Several sets of example problems were demonstrated, ranging from simple models having exact solutions to more complicated applications illustrating global/local analysis. The cantilever beam and circular shaft models showed that the interface elements provide the exact solutions for conforming meshes and very close answers for non–conforming meshes. The Scordelis–Lo roof showed the use of interface elements on a curved surface, and the plate with hole model showed that the interface elements could be used efficiently for global/local analysis, using more elements in the area of interest without having to transition to the model boundaries. The local area in that model was removed and replaced with a more refined mesh.

It is important to note that the interface elements provide a tool for connecting dissimilar meshes, but they do not increase the accuracy of the mesh. As with any interface formulation, the hybrid variational technology, which imposes continuity conditions in a weak form, can not increase the accuracy of the adjacent subdomains. For instance, if a single element face on one boundary is connected to several element faces on the other boundary, the analysis is going to be limited to the accuracy of the less accurate subdomain, no matter how good the interface element is. This restriction should be considered when deciding how close to the areas of primary interest to put the interface elements.

6. Acknowledgement

This work was performed in conjunction with NASA Cooperative Agreement NCC1–202, ‘‘Commercialization of NASA Interface Technology,’’ signed October 18, 1994.

7. References

1. J.E. Schiermeier, J.M. Housner, J.B. Ransom, M.A. Aminpour, and W.J. Stroud, ‘‘The Application of Interface Elements to Dissimilar Meshes in Global/Local Analysis,’’ presented at the MSC 1996 World Users’ Conference, Newport Beach, California, June 3–7, 1996.
2. M.A. Aminpour, J.B. Ransom, and S.L. McCleary, ‘‘Coupled Analysis of Independently Modeled Finite Element Subdomains,’’ presented at the AIAA/ASME/ASCE/AHS/ASC 33rd Structures, Structural Dynamics, and Materials Conference, Dallas, Texas, April 13–15, 1992.
3. J.B. Ransom, S.L. McCleary, and M.A. Aminpour, ‘‘A New Interface Element for Connecting Independently Modeled Substructures,’’ presented at the AIAA/ASME/ASCE/AHS/ASC 34th Structures, Structural Dynamics, and Materials Conference, La Jolla, California, April 19–21, 1993.
4. M.A. Aminpour, J.B. Ransom, and S.L. McCleary, ‘‘A Coupled Analysis Method for Structures with Independently Modelled Finite Element Subdomains,’’ *International Journal for Numerical Methods in Engineering*, Vol. 38, pp. 3695–3718 (1995).
5. J.M. Housner, M.A. Aminpour, C.G. Dávila, J.E. Schiermeier, W.J. Stroud, J.B. Ransom, and R.E. Gillian, ‘‘An Interface Element for Global/Local and Substructuring Analysis,’’ presented at the MSC 1995 World Users’ Conference, Los Angeles, California, May 8–12, 1995.
6. M.A. Aminpour and T. Krishnamurthy, ‘‘A Two–Dimensional Interface Element for Multi–Domain Analysis of Independently Modeled Three–Dimensional Finite Element Meshes,’’ presented at the AIAA/ASME/ASCE/AHS/ASC 38th Structures, Structural Dynamics and Materials Conference, Kissimmee, Florida, April 7–10 (1997).
7. ‘‘MSC and NASA Agreement to Include NASA Technology in MSC/NASTRAN,’’ *MSC/WORLD*, Vol. V, No. 1, pp. 23–24 (February 1995).
8. MSC/NASTRAN Quick Reference Guide Version 70.5, The MacNeal–Schwendler Corporation, Los Angeles, California (to be published).
9. R.H. MacNeal and R.L. Harder, ‘‘A Proposed Standard Set of Problems to Test Finite Element Accuracy,’’ *Finite Elements in Analysis and Design*, Vol. 1, pp. 3–20 (1985).
10. R.J. Roark and W.C. Young, *Formulas for Stress and Strain*, Fifth Edition, McGraw–Hill, Inc., New York (1975).